Delft University of Technology

Identification of iron and sulfate release processes during riverbank filtration using chemical mass balance modeling

An, Seongnam; Kang, Peter K.; Stuyfzand, Pieter J.; Lee, Woonghee; Park, Saerom; Yun, Seong Taek; Lee, Seunghak

DOI
10.1007/s10653-021-00850-0

Publication date
2021

Document Version
Accepted author manuscript

Published in
Environmental Geochemistry and Health

Citation (APA)
An, S., Kang, P. K., Stuyfzand, P. J., Lee, W., Park, S., Yun, S. T., & Lee, S. (2021). Identification of iron and sulfate release processes during riverbank filtration using chemical mass balance modeling. *Environmental Geochemistry and Health*, *43*(9), 3583-3596. https://doi.org/10.1007/s10653-021-00850-0

Important note
To cite this publication, please use the final published version (if applicable).
Please check the document version above.

Copyright
Other than for strictly personal use, it is not permitted to download, forward or distribute the text or part of it, without the consent of the author(s) and/or copyright holder(s), unless the work is under an open content license such as Creative Commons.

Takedown policy
Please contact us and provide details if you believe this document breaches copyrights.
We will remove access to the work immediately and investigate your claim.

This work is downloaded from Delft University of Technology.
For technical reasons the number of authors shown on this cover page is limited to a maximum of 10.

Identification of iron and sulfate release processes during riverbank filtration using chemical mass balance modeling

Seongnam An[a,b], Peter K. Kang[c], Pieter J. Stuyfzand[d,g], Woonghee Lee[c], Saerom Park[e], Seong-Taek Yun[b], Seunghak Lee[a,f,†]

[a] Water Cycle Research Center, National Agenda Research Division, Korea Institute of Science and Technology (KIST), Seoul 02792, Korea

[b] Department of Earth and Environmental Sciences, Korea University, Seoul 136-701, Korea

[c] Department of Earth and Environmental Sciences, University of Minnesota, Minneapolis, MN, 55455, USA

[d] KWR Watercycle Research Institute, PO Box 1072, 3430 BB Nieuwegein, The Netherlands

[e] Urban Water Circulation Research Center, Department of Land, Water and Environment Research, Korea Institute of Civil Engineering and Building Technology (KICT), Gyeonggi-do 10223, South Korea

[f] Graduate School of Energy and Environment (KU-KIST GREEN SCHOOL), Korea University, Seoul 02841, Korea

[g] Technical University Delft, Faculty of Civil Engineering and Geoscience, Delft, Netherlands

† Corresponding author: seunglee@kist.re.kr, tel.: +82-2-958-5817 (S. Lee)

Abstract

Various hydrogeochemical processes can modify the quality of river water during riverbank filtration (RBF). Identifying the subsurface processes responsible for the bank-filtered water quality is challenging, but essential for predicting water quality changes and determining the necessity of post-treatment. However, no systematic approach for this has been proposed yet. In this study, the subsurface hydrogeochemical processes that caused the high concentrations of total iron (Fe) and sulfate (SO_4^{2-}) in the bank-filtered water were investigated at a pilot-scale RBF site in South Korea. For this purpose, water quality variations were monitored in both the extraction well and the adjacent river over five months. The volumetric mixing ratio between the river water and the native groundwater in the RBF well was calculated to understand the effect of mixing on the quality of water from the well, and to assess the potential contribution of subsurface reactions to water quality changes. To identify the subsurface processes responsible for the evolution of Fe and SO_4^{2-} during RBF, an inverse modeling based on the chemical mass balance was conducted using the water quality data and the calculated volumetric mixing ratio. The modeling results suggest that pyrite oxidation by abundant O_2 present in an unsaturated zone could be a primary process explaining the evolution of total Fe and SO_4^{2-} during RBF at the study site. The presence of pyrite in the aquifer was indirectly supported by iron sulfate hydroxide ($Fe(SO_4)(OH)$) detected in oxidized aquifer sediments.

Keywords: Riverbank filtration, iron, sulfate, inverse modeling, chemical mass balance

1. Introduction

Surface water quality deterioration, accelerated by climate change, has encouraged many countries to adopt the bank filtration as a cost-effective pretreatment step in drinking water supplies (Delpla et al., 2009; Sprenger et al., 2011). European countries like Germany, the Netherlands, and Switzerland have relied on bank-filtered water as one of their primary drinking water resources since the 1900s (Sprenger et al., 2017). Recently, South Korea also started to operate an RBF system for treating undesirable substances in the river water such as green algae (Lee et al., 2009; Lee et al., 2012). The general RBF practice consists of a water extraction through wells installed adjacent to a river, which forces the surface water to flow through the subsurface aquifer towards the extraction wells (Ray et al., 2008; Ghodeif et al., 2016). During this process, the concentration of contaminants in the river water can be reduced by subsurface attenuation mechanisms such as mixing, filtration, sorption, and biodegradation (Schwarzenbach et al., 1983; Stuyfzand 1989; Ray et al., 2002; Bertelkamp et al., 2014).

The removal of different organic contaminants by bank filtration has been investigated in many studies (Grunheid et al., 2005; Maeng et al., 2011; Bertelkamp et al., 2014). However, our knowledge on the behavior of inorganic species during the bank filtrations is quite limited. Unusual concentration patterns of inorganic species are sometimes detected in bank-filtered water, which require a geochemical process-based explanation. For example, some RBF systems along the Nile river (Ghodeif et al., 2018) were found to accelerate the release of iron (Fe) and manganese (Mn), which worsened the quality of bank-filtered water (Massmann et al., 2004; Paufler et al., 2018).

Among the inorganic species found in bank-filtered water, Fe has drawn the most attention from researchers (Ray, 2002; Kedziorek et al., 2009; Othman et al., 2015; Grischek & Paufler, 2017). Although Fe is non-toxic, its presence could be associated with that of toxic metals in the filtrate because some Fe minerals in the aquifer might contain Mn, arsenic (As), nickel (Ni), and zinc (Zn) as trace elements (Dowling et al., 2002; Lorenzen et al., 2010; Xie et al., 2015). In addition, Fe precipitates may clog the wells and the aquifer porous network, thereby reducing the overall efficiency of RBF systems (Antoniou et al., 2012; Grischek et al., 2017). Therefore, understanding Fe-related geochemical reactions during RBF is very important to adequately manage RBF systems, both in terms of water quality and quantity aspects.

A recent study (Farnsworth et al., 2011) summarized the major geochemical processes related to Fe behavior during RBF, including the microbially mediated reduction near the riverbank and the oxidation around extraction wells. However, the relative contributions of each process to the final Fe concentration in the bank-filtered water remains unknown although it is essential for predicting water quality changes and determining the necessity of post-treatment. To the best of our knowledge, no systematic approach for identifying the processes relevant to the water quality change during RBF has been proposed yet possibly due to the large uncertainty in the subsurface mineral distributions and the complexity of multiple reactions involved. One way to identify and quantify the inorganic geochemical reactions during RBF is the inverse modeling technique based on the chemical mass balance (Stuyfzand, 2010). In this approach, the molar concentrations of inorganic species in the surface water and the native groundwater are compared with those in the bank-filtered water to determine the most likely combination of subsurface geochemical reactions which best explains the inorganic compositions in bank-filtered water (Antoniou et al., 2012; Stuyfzand, 2006; Stuyfzand, 2006a). As a few examples, Stuyfzand (2006a) employed REACTION+, a chemical mass balance model working in an Excel® spreadsheet, to quantify the extent of hydro-geochemical reactions at the water-sediment interface. Using the same model, Antoniou et al. (2012) identified the major geochemical reactions during aquifer storage and recovery (ASR) in a confined aquifer.

In this study, we focused on a pilot-scale RBF site in the Nakdong river delta in South Korea. During the operation of the RBF facility, Fe and sulfate (SO_4^{2-}) concentrations at the extraction wells increased to the values significantly beyond those that could be estimated from the simple volumetric mixing of river water and native groundwater. This implies that the subsurface reactions during RBF must have occurred. In this study, we aimed to identify the subsurface geochemical reactions responsible for the evolution of Fe and SO_4^{2-} during RBF, and to quantify their relative contributions to the quality of bank-filtered water. For this purpose, we monitored the evolution of water quality at the extraction wells, calculated the volumetric mixing of infiltrated river water and native groundwater in the aquifer, and performed the REACTION+ modeling with the observed data. In addition, we investigated the mineralogy of the aquifer sediments to confirm the presence of the reactive minerals responsible for the process that the REACTION+ modeling indicated as the most plausible.

2. Materials and methods

2.1. Study site and sample collection

The pilot-scale RBF system is located in the Nakdong river delta in southeastern Korea (Fig. S1(a)). The study site has a geological profile of top soil (0–0.8 m), sand layer (0.8–9.6 m), and silty clay layer (9.6–25.8 m), with the groundwater level located at 1.5 m below the ground surface (Ko et al., 2016; Lee et al., 2020). The extraction well is installed 15.2 m away from the riverside and is screened from 8.0 to 9.0 m below the ground surface (Fig. S1(b)). Throughout the total 134 days of well operation (from May to October 2016), the pumping rate was 500 m^3/day during the first 80 days and then decreased to 250 m^3/day for the next 55 days (Fig. S2). Intermittent stops of the pumping system occurred particularly after 60 days from the beginning of the well operation. The bank-filtered water and river water were collected periodically in 50-mL polypropylene tubes at the extraction well and at the riverside, respectively. Samples for analyzing the main constituents were filtrated in the field using a 0.45 μm membrane filter, and transported to the laboratory in a cool box at around 4℃. In particular, the samples for cation analysis were acidified with 0.35 mL HNO_3 (65%) after filtration. A soil sample was collected within the sand layer, 5.5 m below the ground surface and 7 m away from the riverside in the direction of the extraction well, to estimate the mineralogical composition of the aquifer sediments.

2.2. Analytical methods

The pH, dissolved oxygen (DO), oxidation-reduction potential (ORP), electrical conductivity (EC), and temperature were measured on-site using a portable multi-meter (YSI-556 Multi Probe System, YSI) in a flow cell. Cation concentrations (Na^+, Ca^{2+}, K^+, Mg^{2+}, Zn^{2+}, total Fe, and total Mn) were determined by inductively coupled plasma optical emission spectroscopy (ICP-OES, Agilent 730). Anion concentrations (Cl^-, NO_3^- and SO_4^{2-}) were analyzed by ion chromatography (IC, Dionex ICS-1000) equipped with an IonPac AS23 column. Duplicate samples were prepared for both of ICP and IC analyses, and the discrepancy in the charge balances of cation and anion species was ranged in 2~5 %. The bicarbonate (HCO_3^-) concentration was determined by titration (Hem, 1985; Hesse, 1971; Jalali et al., 2009; Neal, 2001; Pauss et al., 1990) with 0.1 N HCl as the acid titrant. DOC was analyzed using a total organic carbon analyzer (TOC-L, Shimadzu) in the DOC mode. The mineralogical composition of the sediment sample from the aquifer was characterized by X-ray diffraction (XRD) using D8 Advance (Lynxeye) with CuKα 1 radiation at 40 kV-40 mA (range: 3–90°, speed: 2 °/min, step: 0.02°).

2.3. Calculating the volumetric mixing ratio of river water and native groundwater

We conducted flow and transport modeling to obtain the volumetric mixing ratio of river water and native groundwater. The mixing ratio allows us to estimate the conservative ion concentrations in the bank-filtered water from those of river water and native groundwater. The steady state groundwater flow field was simulated using MODFLOW (Preconditioned Conjugate Gradient Package 2 (PCG2) solver). ~~The extraction rate of the pumping well was varied according to the actual field operation (500 m^3/day for the first 80 days, then 250 m^3/day).~~The total simulation time was set to 134 days (May 26th, 2016 through Oct 7th, 2016, 134 days in total), with a time step of 1 day. A constant head condition was set to all boundaries, and the regional groundwater flow was assumed to be negligible. The hydraulic conductivity was fixed to 6.5 m/day that was a calibrated value to fit the field-measured hydraulic head (Lee et al., 2020). Using the obtained flow field, a backward particle tracking simulation was performed using PMPATH (Chiang and Kinzelbach, 1994). Five hundred particles were initially deployed at the pumping well, and the travel time of each particle from the well to the domain boundaries was measured. At each time step, the number of particles that reached the river water was counted and divided by the total particle number, thus obtaining the mixing ratio. The relative number of particles that reach the river water is proportional to the volume of river water in the pumping well, so the ratio of the accumulated particle number to the total particle number indicates the volumetric mixing ratio of river water to bank-filtered water.

Using the volumetric mixing ratio, the expected concentrations of conservative tracers at the pumping well can be calculated. The concentration of a conservative ion in the bank-filtered water (C) can be calculated by the following equation:

$$\mathrm{C}\ (\mathrm{mg/L}) = C_G \times r_G + C_S \times r_S \qquad (1)$$

Where, C_G is the concentration in ambient groundwater (mg/L), r_G is the volumetric fraction of ambient groundwater in the bank-filtered, mixed water, C_S is the concentration in the river water (mg/L), and r_S is the volumetric fraction of river water in the bank-filtered, mixed water.

2.4. Chemical mass balance modeling using REACTION+

For identifying and quantifying the geochemical reactions that affect the total Fe and SO_4^{2-} concentrations at the study site, we conducted an inverse modeling using a chemical mass balance model called REACTIONS+ (Version 7, Stuyfzand, 2011). Potential geochemical reactions that can occur during RBF are comprehensively considered in REACTION+ calculation as listed in Table S1 (Stuyfzand, 1998a). REACTION+ quantifies the geochemical reactions by taking into account the differences between the input and the output concentrations of each dissolved component while considering the redox sequences for determining the priority of various reactions with the default settings on the mineral dissolutions of, for example, gypsum ($CaSO_4$), barrite ($BaSO_4$), siderite ($FeCO_3$), gibbsite ($Al(OH)_3$), halite (NaCl), and dolomite ($CaMg(CO_3)_2$). In this regard, a convective transport of O_2 and CO_2 from the unsaturated zone to the unconfined aquifer, a nitrification, and a DOC oxidation by O_2 and NO_3^- are considered first as the initial processes in REACTION+, which are followed by redox and dissolution processes in order (see Table S1). The chemical composition of river water and native groundwater are taken as the model input, which include DO, pH, temperature, DOC, cations and anions, whereas those of the bank-filtered water as the model output. Ambient groundwater is considered as the single initial contributor of bank-filtered water. Since pH and HCO_3^- are not auto-balanced in REACTION+, these are taken as the final calibration terms to evaluate the reliability of the resulting mass balance.

Among the hydrogeochemical reactions consider in the REACTION+, the reactions relevant to total Fe and SO_4^{2-} during RBF are separately summarized again in Table 1. As for the sequence of the redox reactions in Table 1, the pyrite oxidation by O_2 is considered first. The total Fe concentration derived from this reaction (Table 1(a)) is determined by calculating the equivalent molar concentration to that of SO_4^{2-} observed in the bank-filtered water. The molar concentration of SO_4^{2-} generated by the O_2 oxidizing pyrite is determined by considering the oxygen supply given as the input (DO in the river water and the native groundwater) and the oxygen consumption by the initial DOC oxidation in the model. The total Fe concentration attributed to the NO_3^- oxidizing pyrite is determined by calculating the equivalent molar concentration to that of NO_3^- that decreased during RBF through the reaction equation in Table 1(b). The remaining fraction of the measured Fe after being assigned to the products of pyrite oxidation, is designated to be generated by the microbially mediated $Fe(OH)_3$ reduction (Table 1(c)). Dissolution processes (Table 1(d) and (e)) can be optionally included by considering field conditions such as the chemical composition of aquifer sediments, the fluctuation of groundwater table, and pH, etc.

Table 1. Hydrogeochemical processes relevant to the evolution of total Fe and SO_4^{2-} concentrations during RBF

Process		Reaction equation
Redox	Pyrite oxidation by O_2	(a) $3.75O_2 + FeS_2 + 4HCO_3^- \rightarrow Fe(OH)_3 + 2SO_4^{2-} + 4CO_2 + 0.5H_2O$
	Pyrite oxidation by NO_3	(b) $2.8NO_3^- + FeS_2 + 0.8\,CO_2 + 0.4H_2O \rightarrow Fe^{2+} + 2SO_4^{2-} + 0.8HCO_3^- + 1.4N_2$
	$Fe(OH)_3$ reduction	(c) $Fe(OH)_3 + 0.25CH_2O + 1.75CO_2 \rightarrow Fe^{2+} + 2HCO_3^- + 0.75H_2O$
Dissolution	Gypsum	(d) $CaSO_4 \cdot 2H_2O \leftrightarrow Ca^{2+} + SO_4^{2-}$

Siderite	(e) $FeCO_3 + CO_2 + H_2O \leftrightarrow Fe^{2+} + 2HCO_3^-$

3. Results and discussion

3.1. Temporal changes of dissolved ion concentrations in bank-filtered water

3.1.1 Field observations

Table 2 summarizes the average water quality data of river water, native groundwater, and bank-filtered water from the pumping well. Detailed temporal changes of river and bank-filtered water quality are reported in Tables S2 and S3, respectively, in the supplementary data file.

Table 2. Average water quality of river water, native groundwater, and bank-filtered water

	River water [a] (± standard deviation)	Native Groundwater [b] (± standard deviation)	Bank-filtered water [c] (± standard deviation)
Temp. (°C)	26.118 (±3.916)	20.103	21.31 (±0.710)
pH	8.11 (±0.539)	7.016	7.19 (±0.171)
ORP (mV)	42.8 (±41.391)	-81.4 (±70.3)	-14.13 (±39.726)
EC (mS/cm)	0.318 (±0.182)	4.407	1.168 (±0.043)
O_2 (mM)	0.247 (±0.066)	0.071	0.01 (±0.007)
Total Fe (mM)	N.D.	0.358 (±0.145)	N.A. (see Table S3)
Total Mn (mM)	N.D.	0.024 (±0.008)	0.009 (±0.006)
Na^+ (mM)	0.667 (±0.332)	15.912 (±1.179)	5.051 (±0.585)
Ca^{2+} (mM)	0.562 (±0.166)	3.535 (±0.894)	1.221 (±0.437)
Mg^{2+} (mM)	0.212 (±0.037)	3.008 (±0.265)	1.466 (±0.025)
K^+ (mM)	0.111 (±0.024)	0.740 (±0.004)	0.407 (±0.043)
SO_4^{2-} (mM)	0.212 (±0.064)	0.134 (±0.035)	N.A. (see Table S3)
Cl^- (mM)	0.563 (±0.356)	18.177 (±1.424)	4.405 (±0.387)
NO_3^- (mM)	0.105 (±0.028)	0.019 (±0.018)	N.D.
HCO_3^- (mM)	0.896 (±0.172)	8.207 (±0.476)	4.915 (±0.370)
DOC (mM)	0.169 (±0.041)	0.412 (±0.053)	0.625 (±0.273)

N.D.: Not detected; N.A.: Not available; [a] Mean value from day 1 to day 134 (May 27th – Oct 7th, 2016); [b] Mean value for the first two days (May 27th–28th, 2016, before the mixing of native groundwater with the intruded river water); [c] Mean value from day 64 to day 134 (July

29th – Oct 7th, 2016, when the bank-filtered water has a stable mixing ratio of river water and native groundwater)

The in-situ measurements revealed that DO and ORP of river water were compatible with oxidizing conditions (i.e., 5–10 mg/L for DO, and 10–120 mV for ORP), while those of the ambient groundwater with reducing conditions (i.e., 0.9–1.49 mg/L for DO, and -151.7– -11.1 mV for ORP). This can be also seen from the different concentrations of redox-sensitive parameters such as Mn and NO_3^-. In general, the ion concentrations in the bank-filtered water were higher than those in the river water due to (i) the mixing with the native groundwater, and (ii) the various water-rock interactions underwent by the bank-filtered water. The DOC concentrations in every water sample fell in the range of typical groundwater (0.1–1 mM) (Appelo and Postma, 2004). However, the DOC in the bank-filtered water was higher than those of the river and the native groundwater, which is abnormal since DOC is known to be readily oxidized by O_2 and NO_3^- present or introduced in the aquifer during RBF. We believe that this might be caused by the presence of organic matter in the subsurface around the pumping well.

3.1.2 Calculation based on the volumetric mixing ratio

The relative volumetric ratios of the river water and the native groundwater in the bank-filtered water are shown in Fig. 1. At the beginning of the operation, only native groundwater was present in the bank filtered water. However, the contribution of river water in the filtered water rapidly increased and it reached 80 % at the end of the operation.

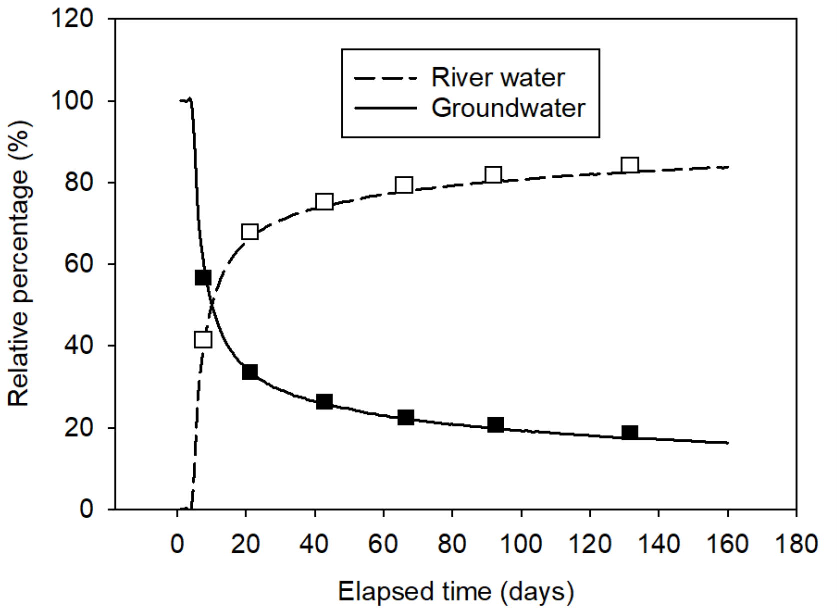

Fig. 1. Relative volumetric ratios of river water and ambient groundwater in the bank-filtered water. The square marker indicates the day when water quality data were collected

Assuming the non-reactive (conservative) transport of dissolved ions and no additional hydrogeochemical reactions during RBF, the ion concentrations in the bank-filtered water were calculated using Eq. (1) according to the relative volumetric ratios of river water and native groundwater (see Fig. 1). The initial native groundwater quality was assumed as the average water quality at the pumping well during the first two days of operation (May 27th and 28th, 2016; see Table S3) when the river water intrusion was negligible. The PMPATH calculation gives that the first arrival of river water to the pumping well occurs on day 5. The calculated and measured ion concentrations in the bank-filtered water are shown in Fig. 2. To compare the degree of discrepancy between the ions with different concentration ranges, the mean deviation of the normalized concentrations was calculated for each ion by the following equation:

$$\text{Mean deviation} = \frac{\sum_{i=1}^{n}\left(\frac{y_i}{C_0} - \frac{x_i}{C_0}\right)}{n} \qquad (2)$$

Where, n is the number of data for an ion, y_i is the measured concentration of an ion, x_i is the calculated concentration of an ion based on the volumetric mixing, and C_0 is the initial concentration of an ion in the native groundwater.

As shown in Fig. 2, the concentration of an ion in the bank-filtered water generally decreased with time as the contribution of river water (having lower ion concentrations than the native groundwater) increased. Mean deviations for Na^+, Ca^{2+}, and Cl^- remained low (in the range of -0.1 to 0.1), implying that the concentration of these ions could be properly predicted by considering only the mixing effect (see Fig. 2(a)). In particular, Cl^- (conservative tracer) showed the least mean error among the considered ions, validating the mixing ratio calculated by the flow model. Interestingly, the calculated concentrations of Ca^{2+} were generally higher than the measured values, while the opposite was true in the case of Na^+. This might be explained with the exchange of divalent Ca^{2+} for monovalent Na^+ (Appelo and Postma, 2004) in the aquifer sediment during RBF.

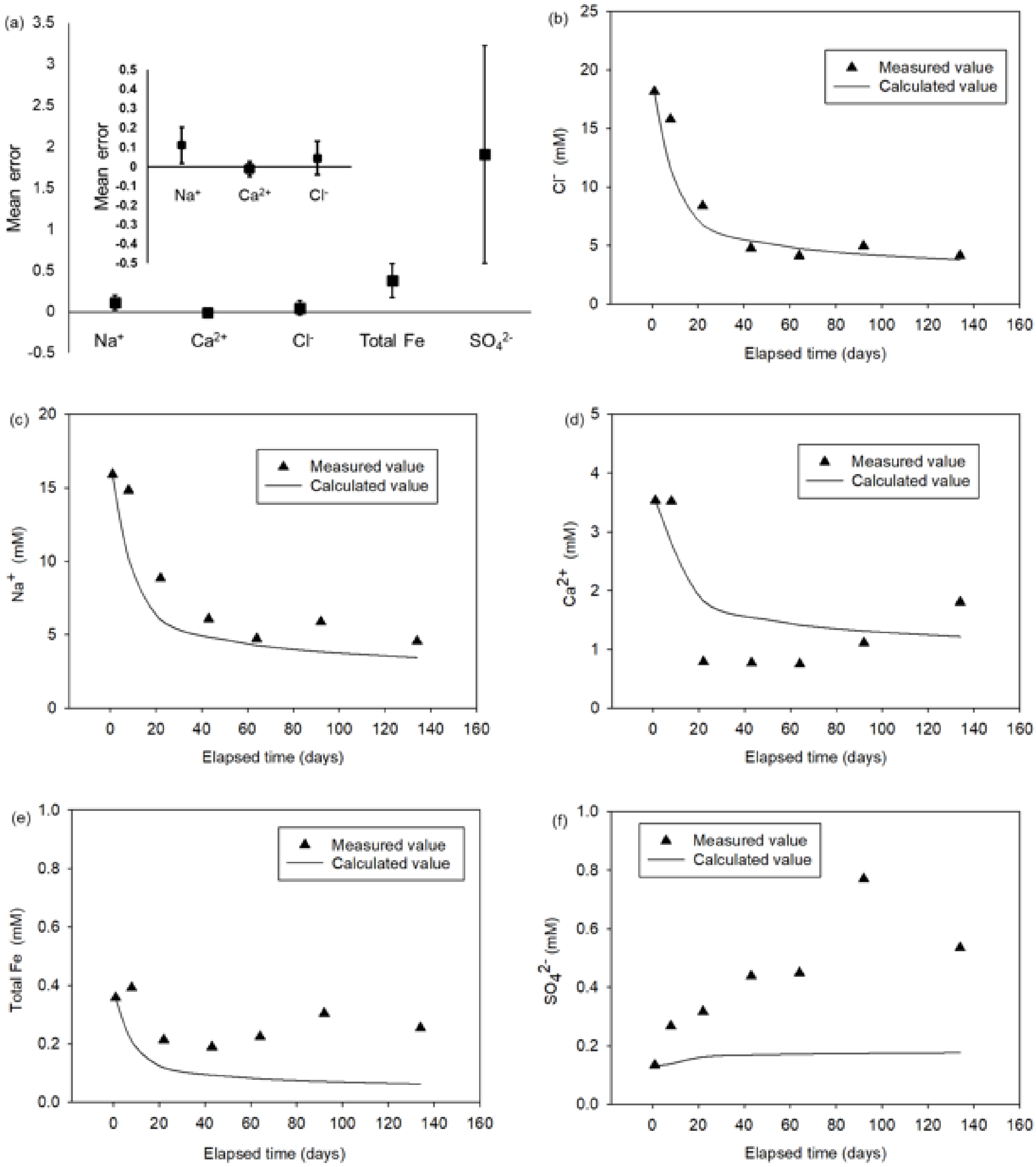

Fig. 2. Differences between measured and calculated ion concentrations summarized as (a) the mean errors of normalized concentrations of each ion, shown for: (b) Cl^-, (c) Na^+, (d) Ca^{2+}, (e) total Fe, and (f) SO_4^{2-}

While the results for Na^+, Ca^{2+}, and Cl^- were satisfactory, the mean errors for total Fe and SO_4^{2-} were significantly high. The total Fe concentration decreased in the early period of well operation possibly because of mixing, as was the case for Na^+, Ca^{2+}, and Cl^-, but subsequently increased (see Fig. 2(e)) even though the dilution effect became more significant over time (see Fig. 1). The temporal change of SO_4^{2-} concentration shows a pattern similar to that of total Fe, except for the gradual increase in the early period, which could be attributed to the slightly higher SO_4^{2-} concentrations in the river water (0.192–0.274 mM) than in the native groundwater (0.099–0.169 mM). This suggests that some hydrogeochemical reactions involving Fe and SO_4^{2-} should have occurred during RBF at the site.

3.2. REACTION+ modeling

In order to assess the relative contribution of various subsurface reactions to the total Fe and SO_4^{2-} concentrations in the bank-filtered water, a chemical mass balance analysis was conducted using REACTION+. In this approach, two assumptions were made: (1) that all reactions are in the steady state during RBF operation, and (2) that the minerals involved in the reactions are spatially homogeneous in the aquifer.

3.2.1. Hydrogeochemical reactions responsible for total Fe evolution during RBF

As summarized in Table 1, the subsurface reactions relevant to the total Fe evolution during RBF include $Fe(OH)_3$ reduction, pyrite oxidation, and siderite dissolution. Among these reactions, siderite ($Fe_{(1-x)}Mn_xCO_3$) dissolution was neglected in this estimation considering the aquifer environmental conditions. Siderite dissolution is known to be favored only at the pH below 5.2; therefore, this reaction should be limited at typical groundwater pH of 6–8 (Walter et al., 1994). Duckworth et al. (2004) also demonstrated that siderite hardly dissolved at a pH of 6–8 due to the presence of a $Fe(OH)_3$ coating that formed on its surface by siderite oxidation. Moreover, siderite was found to have a solubility product constant (K_{sp}) of $10^{-10.12} – 10^{-11.2}$ in the temperature range of 17–25 °C (which is even slightly higher than the typical aquifer condition), corresponding to a solubility of approximately 6.09×10^{-6} mol/L (0.013 mM) (Jensen et al., 2002; Benezeth et al., 2009). The ionic balance between Ca^{2+} and HCO_3^- (i.e., $2\times[Ca^{2+}] / [HCO_3^-] \approx 0.86$) in the native groundwater also supports the exclusion of siderite dissolution from the modeling.

The results of the chemical mass balance analysis for total Fe are shown in Fig. 3(a) and 3(b). The O_2 supply from the unsaturated zone into the groundwater was set to zero in this analysis for clarifying the potential effect of oxygen originally dissolved in the river water which was given as the model input. The calculated concentration of total Fe, which is the sum of the Fe concentrations expected from pyrite oxidation and $Fe(OH)_3$ reduction, is comparable with the values measured in the field (Fig. 3(a)). Among the considered reactions, $Fe(OH)_3$ reduction was shown to dominate the total Fe release during RBF (except on the 43rd day, see Fig. 3(b)), which is consistent with the findings from previous studies (Farnsworth et al., 2011; Ko et al., 2016). Pyrite oxidation by O_2 and NO_3^- was also found to contribute to the total Fe evolution in the bank-filtered water. This could be due to the constant O_2 supply from the river water (> 5 mg/L) during RBF. Some researchers reported the possible release of metals such as As, Fe and Mn contained in the aquifer minerals triggered by the intrusion of surface water into the aquifer (Anawar et al., 2003; Massmann et al., 2008). The moderate amount of NO_3^- in the river water (0.068–0.144 mM, see Table S2) is also expected to oxidize some pyrite (Engesgaard et al., 1992; Juncher Jorgensen et al., 2009; Zhang et al., 2009). It should be noted that the NO_3^- consumption is priorly considered to be attributed to the pyrite oxidation in REACTION+.

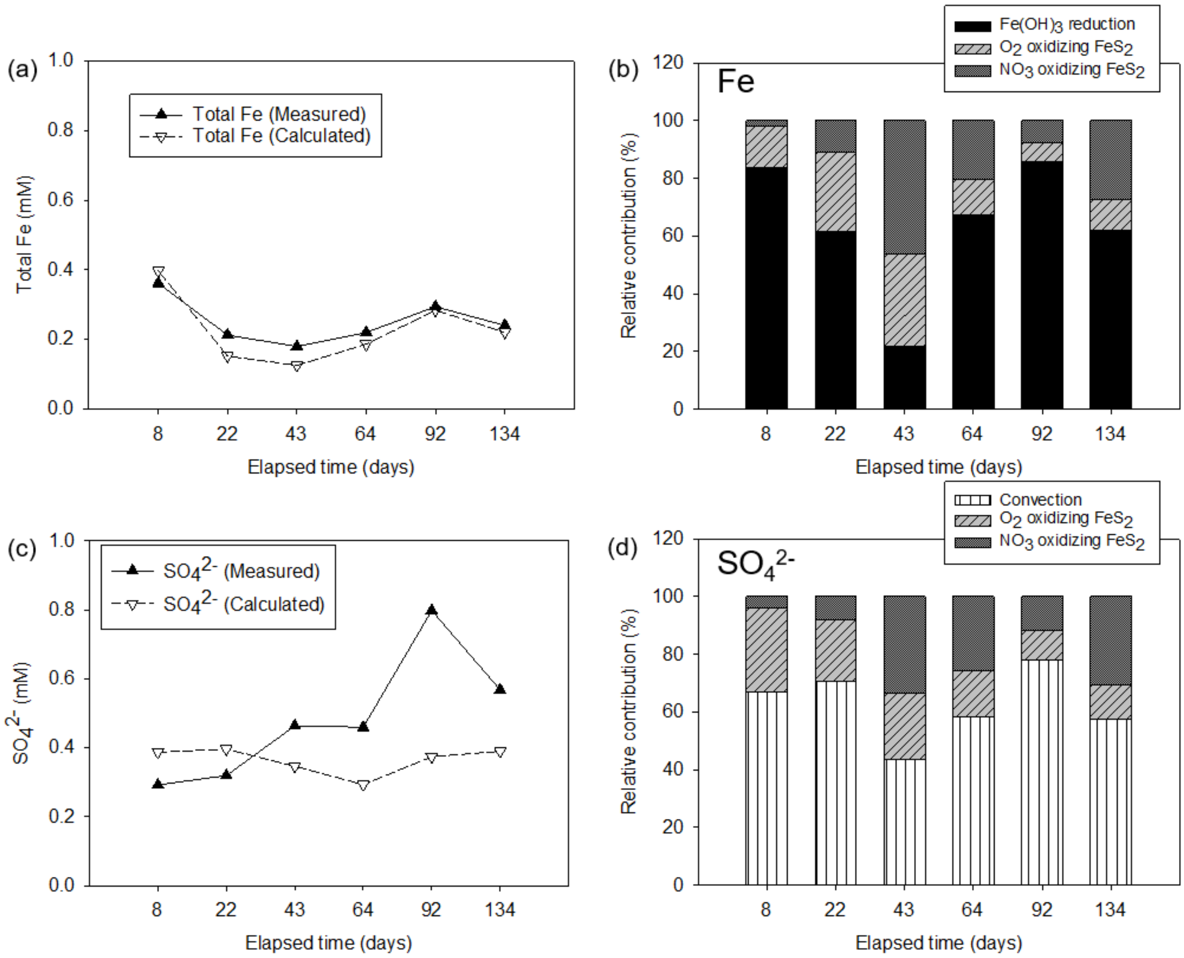

Fig. 3. Results of the REACTION+ model simulation without oxygen supply from the unsaturated zone showing: (a) the calculated total Fe concentrations compared with the measured ones, (b) the relative contributions of different hydrogeochemical processes to the total Fe concentration in the bank-filtered water, (c) the calculated SO_4^{2-} concentrations compared with the measured ones, and (d) the relative contributions of different hydrogeochemical processes to the SO_4^{2-} concentration in the bank-filtered water.

3.2.2. Hydrogeochemical reactions responsible for SO_4^{2-} evolution during RBF

The hydrogeochemical processes evolving SO_4^{2-} in the aquifer during RBF include pyrite oxidation and gypsum dissolution (see Table 1). In our analysis, gypsum dissolution was excluded by presuming the potential gypsum contents in the concerning aquifer. The ion activity product (IAP) calculated from the initial concentrations of Ca^{2+} and SO_4^{2-} in the native groundwater (IAP = $[Ca^{2+}]*[SO_4^{2-}] = 4.38*10^{-7}$) is much lower than the solubility product constant ($K_{sp} = [Ca^{2+}]*[SO_4^{2-}] = 10^{-4.6}$) (Faure, 1998). This indicates that the initial SO_4^{2-} concentration could be as high as 5.012 mM in the presence of gypsum; however, the much lower SO_4^{2-} concentration in the ambient groundwater (0.134 mM) should imply little gypsum content in the aquifer minerals. It is also supported by the saturation index (SI= log(IAP/Ksp)= -1.76) of gypsum.

The results of the chemical mass balance analysis for SO_4^{2-} are shown in Fig. 3(c) and 3(d). In this analysis, the oxygen supply from the unsaturated zone into the groundwater was assumed to be zero. The calculated concentrations do not match well with the measured values, particularly beyond day 64 (Fig. 3(c)), implying that the hydrogeochemical processes in the field have not been properly captured in the modeling. In the analysis, however, the evolution of SO_4^{2-} in the bank-filtered water was found to be mainly attributed to convection and pyrite oxidation by O_2 and NO_3^- (Fig. 3(d)). Convection had its significance in this modeling due to the higher concentrations of SO_4^{2-} in the river water compared to the native groundwater during RBF. The contribution of pyrite oxidation to the SO_4^{2-} concentrations could be explained in the same manner as that for the total Fe evolution.

3.3. Incorporation of O2 diffusion from the unsaturated zone into the groundwater in the modeling

The effect of O_2 diffusion from the unsaturated zone into the groundwater on the water quality change during RBF has not been clearly demonstrated in the previous studies. However, as shown in the model setup with no O_2 supply (see section 3.2), the calibration terms of pH and HCO_3^- could not be calculated in many cases (see Table 3), and significant discrepancies existed between the calculated and measured SO_4^{2-} concentrations. To reduce these discrepancies, the model setup was adjusted by taking specific field conditions into account.

Table 3. Calibration terms of pH and HCO_3^- measured in the field and calculated by REACTION+

Days after starting the RBF system		8	22	43	64	92	134
Without oxygen supply from the unsaturated zone							
pH	measured	7.15	7.00	7.02	7.01	7.02	7.03
	calculated	N.A.	N.A.	N.A.	N.A.	7.08	N.A.
HCO_3^- (mM)	measured	7.13	5.10	4.55	4.50	4.85	5.40
	calculated	6.11	3.16	3.95	3.56	5.40	5.08
With oxygen supply from the unsaturated zone							
pH	measured	7.15	7.00	7.02	7.01	7.02	7.03
	calculated	6.75	6.98	6.99	6.97	6.98	7.04
HCO_3^- (mM)	measured	7.13	5.10	4.55	4.50	4.85	5.40
	calculated	6.89	4.15	4.32	4.07	4.24	5.61

N.A.: Not Available

First, we noticed that the groundwater level at the study site was 1.5 m below the ground, implying that O_2 diffusion from the atmosphere into the groundwater is preferable. Consequently, the initial condition of O_2 supply during the stable period (without groundwater table fluctuation) in the model was changed to 0.3 mM of which value was determined by considering the O_2 solubility (9 mg/L) at the temperature of shallow subsurface (assumed as 20~22 ºC).

In addition, we identified some events that might have altered the subsurface reaction conditions on day 64, 92 and 134. Particularly, just before day 92 when an abrupt increase in the SO_4^{2-} concentration was observed, the pumping rate of the extraction well decreased from 500 m^3/day to 250 m^3/day (see Fig. S2). Several studies showed that a change in the pumping rate can induce groundwater table fluctuations which may result in excess O_2 diffusion to the groundwater (Williams et al et al., 2000; Massmann et al., 2008; Farnsworth et al., 2011).

Kohfahl et al. (2009) suggested that the air bubbles entrapped in the soil pores due to groundwater table fluctuations might be the most important source of O_2 flux into the groundwater during RBF. Fry et al (1997) reported that the O_2 concentration caused by groundwater table fluctuations could be 28 times higher than O_2 solubility in water (0.3 mM × 28 = 8.4 mM), and Amos et al. (2006) showed that it could vary in the range of 10 ~150 mM within the realm of groundwater table. Therefore, in order to incorporate the sudden decrease in the pumping rate, the O_2 supply in the model increased to 3 mM (10 times higher than that in the stable condition but much lower than the previously reported values) on day 92, even though the actual O_2 supply around the pumping well could not be exactly measured or calculated. Furthermore, the oxygen supply on day 64 and 134 were adjusted to 0.6 mM (twice higher than that in the stable condition) because the pump was temporarily switched off, which could enhance the O_2 dissolution into the groundwater. Farnsworth et al. (2011) showed that on-off cycles of the pumping well could cause groundwater table oscillations at an RBF site. The value of 0.6 mM was determined to be slightly higher than that caused by atmospheric O_2 diffusion into the groundwater (0.3 mM) and to minimize the difference between the measured and calculated calibration terms.

The calibration terms of pH and HCO_3^- calculated in the adjusted REACTION+ run are summarized in Table 3. This time, the terms could be obtained in all cases, and their values were similar to the measured data.

As shown in Fig. 4, the adjusted REACTION+ run provided total Fe and SO_4^{2-} values that describe the trends of measured values better than the values provided by the initial model run (which included the O_2 supply from the unsaturated zone to the aquifer; see Fig. 3(a) and 3(c) with Fig. 4(a) and 4(c)). The reason for the higher discrepancy observed in SO_4^{2-} than in total Fe remains unclear. The adjusted model run suggests that pyrite oxidation by O_2 is the main process responsible for the evolution of both total Fe and SO_4^{2-} (Fig. 4(b) and 4(d)). The effect of pyrite oxidation by NO_3^- was neglected on day 92, possibly because of the initially high O_2 convection into the groundwater. The relative contribution of $Fe(OH)_3$ reduction, which should be the major source of Fe in the native groundwater, decreased as the river water intrusion proceeded. For some cases (on day 43 and 92), the adjusted modeling included the processes that can reduce the dissolved Fe concentration by forming the iron precipitates ($Fe(OH)_3$).

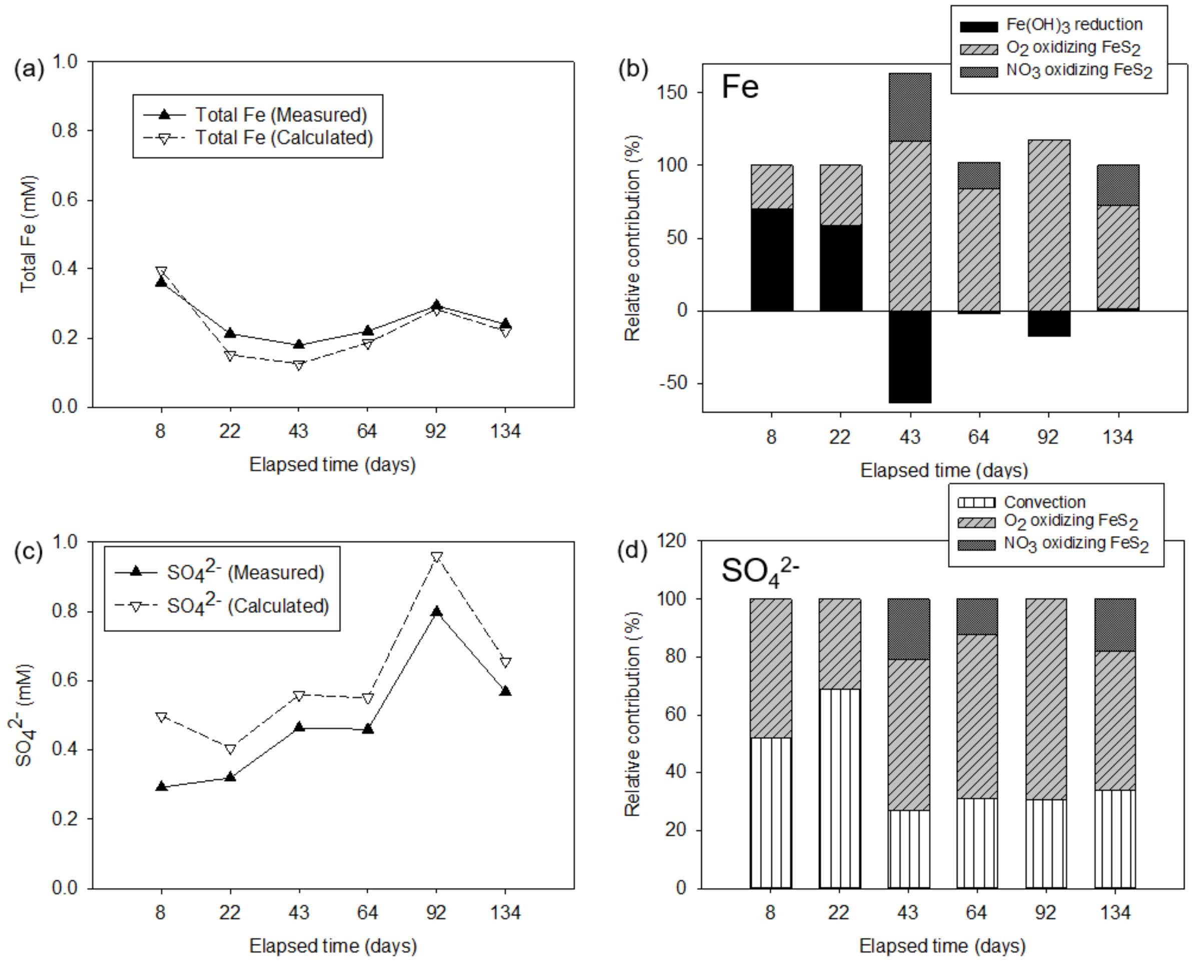

Fig. 4. Results of the adjusted REACTION+ model simulation with oxygen supply from the unsaturated zone showing: (a) the calculated total Fe concentrations compared with the measured ones, (b) the relative contributions of different hydrogeochemical processes to the total Fe concentration in the bank-filtered water, (c) the calculated SO_4^{2-} concentrations

compared with the measured ones, and (d) the relative contributions of different hydrogeochemical processes to the SO_4^{2-} concentration in the bank-filtered water

3.4. Mineralogical analysis of aquifer sediments for confirming the presence of pyrite

The REACTION+ modeling results shown in the previous section suggested that pyrite oxidation by O_2 should be the main contributor to the evolution of total Fe and SO_4^{2-} during RBF at the site. To evaluate the reliability of this result, the mineralogical composition of a sediment sample collected from the aquifer was analyzed, focusing on the presence of pyrite.

Although it has been reported that the pyrite can exist in shallow aquifers (Berner, 1984; Rickard, 1975; Rust, 1935; Sawlowicz, 1993; Wilkin and Barnes, 1997), pyrite was not detected in the aquifer sediment directly. However, iron sulfate hydroxide ($Fe(SO_4)(OH)$) was found (see Fig. S3) which can be considered as the oxidized form of pyrite. Komnitas et al. (1995) and Majzlan et al. (2018) reported that $Fe(SO_4)(OH)$ can be generated from pyrite as a parent mineral by weathering and bacterial oxidation. This might be due to pyrite oxidation under the atmospheric condition to which the sediment sample was exposed during storage and analytical procedures (Moses et al., 1991), and/or the current single specific sampling location despite of the heterogeneous distribution of pyrite in the aquifer.

4. Conclusions

In this study, the subsurface hydrogeochemical reactions responsible for the abnormally high Fe and SO_4^{2-} in the bank-filtered water were identified using the chemical mass balance modeling approach. When the reaction conditions resulting from the site-specific groundwater level and the system operational events were incorporated into the modeling, the results became more reliable with respect to the model calibration terms and the calculated values of Fe and SO_4^{2-}. The model identified the pyrite oxidation by O_2 as the most relevant subsurface process to the evolution of total Fe and SO_4^{2-} during RBF at the study site. Identifying "hidden" subsurface hydrogeochemical processes is critical to various practices such as reactive transport modeling and the design of a water treatment strategy. Reactive transport modeling has been proven effective in many studies to obtain insights into the spatiotemporal evolution of groundwater quality. However, the adequate selection of relevant subsurface processes is a prerequisite for successful reactive transport modeling. The identification of contaminant-releasing mechanisms is also essential for designing a satisfactory subsurface remediation strategy. However, it should be noted that REACTION+ relies upon batch-type equilibrium reactions, and it does not consider the effects of reaction kinetics and transport processes. Combining chemical mass balance modeling used in this study and reactive transport modeling could become a robust framework for comprehensively characterizing water quality changes during RBF. Also, multiple mineralogical analyses of aquifer materials and laboratory experiments can contribute to the improved characterization of the geochemical reactions in the subsurface.

Declarations

Funding: The authors acknowledge support from the Future Research Program (2E30510) funded by the Korea Institute of Science and Technology (KIST), and the Korea Environmental Industry & Technology Institute (KEITI) through the Subsurface Environment Management (SEM) Project (2018002440006) funded by the Korea Ministry of Environment (MOE). PKK also acknowledges the College of Science & Engineering at the University of Minnesota and the George and Orpha Gibson Endowment for its generous support of Hydrogeology, and the Minnesota Environment and Natural Resources Trust Fund as recommended by the Legislative-Citizen Commission on Minnesota Resources (LCCMR).

Conflict of interest/Competing interests: The authors have no relevant financial or non-financial interests to disclose.

Availability of data and material: Not applicable

Code availability: Not applicable

Authors' contributions

Seongnam An: Field monitoring, REACTION+ modeling, Writing – original draft. **Peter K. Kang:** Writing – review & editing. **Pieter J. Stuyfzand:** Review & comment. **Woonghee Lee:** MODFLOW and PMPATH modeling. **Saerom Park:** Review & comment. **Seong-Taek Yun:** Review & comment. **Seunghak Lee:** Funding acquisition, Writing – revision & editing, Project administration.

Ethics approval: Not applicable

Consent to participate: Not applicable

Consent to publication: Not applicable

References

Amos, R. T., & Mayer, K. U. (2006). Investigating the role of gas bubble formation and entrapment in contaminated aquifers: Reactive transport modelling. *Journal of contaminant hydrology*, *87*(1-2), 123-154.

Anawar, H. M., Akai, J., Komaki, K., Terao, H., Yoshioka, T., Ishizuka, T., Safiullah, S., & Kato, K. (2003). Geochemical occurrence of arsenic in groundwater of Bangladesh: sources and mobilization processes. *Journal of Geochemical Exploration*, *77*(2-3), 109-131.

Antoniou, E. A., Van Breukelen, B. M., Putters, B., & Stuyfzand, P. J. (2012). Hydrogeochemical patterns, processes and mass transfers during aquifer storage and recovery (ASR) in an anoxic sandy aquifer. *Applied Geochemistry*, *27*(12), 2435-2452.

Appelo, C. A. J., & Postma, D. (2004). *Geochemistry, Groundwater and Pollution*. CRC press.

Bartak, R., Macheleidt, W., & Grischek, T. (2017). Controlling the formation of the reaction zone around an injection well during subsurface iron removal. *Water*, *9*(2), 87.

Bénézeth, P., Dandurand, J. L., & Harrichoury, J. C. (2009). Solubility product of siderite (FeCO3) as a function of temperature (25–250 C). *Chemical Geology*, *265*(1-2), 3-12.

Berner, R. A. (1984). Sedimentary pyrite formation: an update. *Geochimica et cosmochimica Acta*, *48*(4), 605-615.

Bertelkamp, C., Reungoat, J., Cornelissen, E. R., Singhal, N., Reynisson, J., Cabo, A. J., van der Hoek, J.P., & Verliefde, A. R. D. (2014). Sorption and biodegradation of organic micropollutants during river bank filtration: a laboratory column study. *Water Research*, *52*, 231-241.

Chiang, W. H., & Kinzelbach, W. (1994). PMPATH, An Advective Transport Model for Processing Modflow and Modflow. *Geol Surv Hambg, Germany*.

Dash, R. R., Mehrotra, I., Kumar, P., & Grischek, T. (2008). Lake bank filtration at Nainital, India: water-quality evaluation. *Hydrogeology Journal*, *16*(6), 1089-1099.

Delpla, I., Jung, A. V., Baures, E., Clement, M., & Thomas, O. (2009). Impacts of climate change on surface water quality in relation to drinking water production. *Environment International*, *35*(8), 1225-1233.

Dowling, C. B., Poreda, R. J., Basu, A. R., Peters, S. L., & Aggarwal, P. K. (2002). Geochemical study of arsenic release mechanisms in the Bengal Basin groundwater. *Water Resources Research*, *38*(9), 12-1.

Duckworth, O. W., & Martin, S. T. (2004). Role of molecular oxygen in the dissolution of siderite and rhodochrosite1. *Geochimica et Cosmochimica Acta*, *68*(3), 607-621.

Engesgaard, P., & Kipp, K. L. (1992). A geochemical transport model for redox-controlled movement of mineral fronts in groundwater flow systems: A case of nitrate removal by oxidation of pyrite. *Water Resources Research*, *28*(10), 2829-2843.

Farnsworth, C. E., & Hering, J. G. (2011). Inorganic geochemistry and redox dynamics in bank filtration settings. *Environmental Science & Technology*, *45*(12), 5079-5087.

Faure, G. (1998). *Principles and applications of geochemistry: a comprehensive textbook for geology students*. Prentice Hall.

Fry, V. A., Selker, J. S., & Gorelick, S. M. (1997). Experimental investigations for trapping oxygen gas in saturated porous media for in situ bioremediation. *Water Resources Research*, *33*(12), 2687-2696.

Ghodeif, K., Grischek, T., Bartak, R., Wahaab, R., & Herlitzius, J. (2016). Potential of river bank filtration (RBF) in Egypt. *Environmental Earth Sciences*, *75*(8), 671.

Ghodeif, K., Paufler, S., Grischek, T., Wahaab, R., Souaya, E., Bakr, M., & Abogabal, A. (2018). Riverbank filtration in Cairo, Egypt—part I: installation of a new riverbank filtration site and first monitoring results. *Environmental Earth Sciences*, *77*(7), 270.

Grünheid, S., Amy, G., & Jekel, M. (2005). Removal of bulk dissolved organic carbon (DOC) and trace organic compounds by bank filtration and artificial recharge. *Water Research*, *39*(14), 3219-3228.

Grischek, T., & Paufler, S. (2017). Prediction of iron release during riverbank filtration. *Water*, *9*(5), 317.

Grünheid, S., Amy, G., & Jekel, M. (2005). Removal of bulk dissolved organic carbon (DOC) and trace organic compounds by bank filtration and artificial recharge. *Water Research*, *39*(14), 3219-3228.

Heberer, T., Massmann, G., Fanck, B., Taute, T., & Dünnbier, U. (2008). Behaviour and redox sensitivity of antimicrobial residues during bank filtration. *Chemosphere*, *73*(4), 451-460.

Hem, J. D. (1985). *Study and interpretation of the chemical characteristics of natural water* (Vol. 2254). Department of the Interior, US Geological Survey.

Hesse, P. R. (1971). *A textbook of soil chemical analysis* (No. 631.41 H4).

Hu, B., Teng, Y., Zhai, Y., Zuo, R., Li, J., & Chen, H. (2016). Riverbank filtration in China: A review and perspective. *Journal of Hydrology*, *541*, 914-927.

Jalali, M. (2009). Geochemistry characterization of groundwater in an agricultural area of Razan, Hamadan, Iran. *Environmental Geology*, *56*(7), 1479-1488.

Jensen, D. L., Boddum, J. K., Tjell, J. C., & Christensen, T. H. (2002). The solubility of rhodochrosite (MnCO3) and siderite (FeCO3) in anaerobic aquatic environments. *Applied Geochemistry*, *17*(4), 503-511.

Juncher Jørgensen, C., Jacobsen, O. S., Elberling, B., & Aamand, J. (2009). Microbial oxidation of pyrite coupled to nitrate reduction in anoxic groundwater sediment. *Environmental Science & Technology*, *43*(13), 4851-4857.

Kang, P. K., Bresciani, E., An, S., & Lee, S. (2019). Potential impact of pore-scale incomplete mixing on biodegradation in aquifers: From batch experiment to field-scale modeling. *Advances in Water Resources*, *123*, 1-11.

Kedziorek, M. A., & Bourg, A. C. (2009). Electron trapping capacity of dissolved oxygen and nitrate to evaluate Mn and Fe reductive dissolution in alluvial aquifers during riverbank filtration. *Journal of Hydrology*, *365*(1-2), 74-78.

Kim, K. H., Heiss, J. W., Michael, H. A., Cai, W. J., Laattoe, T., Post, V. E., & Ullman, W. J. (2017). Spatial patterns of groundwater biogeochemical reactivity in an intertidal beach aquifer. *Journal of Geophysical Research: Biogeosciences*, *122*(10), 2548-2562.

Ko, M. S., Cho, K., Jeong, D., & Lee, S. (2016). Identification of the microbes mediating Fe reduction in a deep saline aquifer and their influence during managed aquifer recharge. *Science of the Total Environment*, *545*, 486-492.

Kohfahl, C., Massmann, G., & Pekdeger, A. (2009). Sources of oxygen flux in groundwater during induced bank filtration at a site in Berlin, Germany. *Hydrogeology Journal*, *17*(3), 571.

Komnitsas, K., Xenidis, A., & Adam, K. (1995). Oxidation of pyrite and arsenopyrite in sulphidic spoils in Lavrion. *Minerals Engineering*, *8*(12), 1443-1454.

Lee, J. H., Hamm, S. Y., Cheong, J. Y., Kim, H. S., Ko, E. J., Lee, K. S., & Lee, S. I. (2009). Characterizing riverbank-filtered water and river water qualities at a site in the lower Nakdong River basin, Republic of Korea. *Journal of Hydrology*, *376*(1-2), 209-220.

Lee, E., Hyun, Y., Lee, K. K., & Shin, J. (2012). Hydraulic analysis of a radial collector well for riverbank filtration near Nakdong River, South Korea. *Hydrogeology Journal*, *20*(3), 575-589.

Lee, W., Bresciani, E., An, S., Wallis, I., Post, V., Lee, S., & Kang, P. K. (2020). Spatiotemporal evolution of iron and sulfate concentrations during riverbank filtration: Field observations and reactive transport modeling. *Journal of Contaminant Hydrology*, 103697.

Lorenzen, G., Sprenger, C., Taute, T., Pekdeger, A., Mittal, A., & Massmann, G. (2010). Assessment of the potential for bank filtration in a water-stressed megacity (Delhi, India). *Environmental Earth Sciences*, *61*(7), 1419-1434.

Maeng, S. K., Sharma, S. K., Lekkerkerker-Teunissen, K., & Amy, G. L. (2011). Occurrence and fate of bulk organic matter and pharmaceutically active compounds in managed aquifer recharge: a review. *Water Research*, *45*(10), 3015-3033.

Majzlan, J., Dachs, E., Benisek, A., Plášil, J., & Sejkora, J. (2018). Thermodynamics, crystal chemistry and structural complexity of the Fe (SO4)(OH)(H2O) x phases: Fe (SO4)(OH), metahohmannite, butlerite, parabutlerite, amarantite, hohmannite, and fibroferrite. *European Journal of Mineralogy*, *30*(2), 259-275.

Massmann, G., Pekdeger, A., & Merz, C. (2004). Redox processes in the Oderbruch polder groundwater flow system in Germany. *Applied Geochemistry*, *19*(6), 863-886.

Massmann, G., Nogeitzig, A., Taute, T., & Pekdeger, A. (2008). Seasonal and spatial distribution of redox zones during lake bank filtration in Berlin, Germany. *Environmental Geology*, *54*(1), 53-65.

Moses, C. O., & Herman, J. S. (1991). Pyrite oxidation at circumneutral pH. *Geochimica et Cosmochimica Acta*, *55*(2), 471-482.

Olin Neal, C. (2001). Alkalinity measurements within natural waters: towards a standardised approach. *Science of the Total Environment*, *265*(1-3), 99-113.

Othman, S. Z., Adlan, M. N., & Selamat, M. R. (2015). A study on the potential of riverbank filtration for the removal of color, iron, turbidity and E. coli in Sungai Perak, Kota Lama Kiri, Kuala Kangsar, Perak, Malaysia. *Jurnal Teknologi*, *74*(11), 83-91.

Paufler, S., Grischek, T., Bartak, R., Ghodeif, K., Wahaab, R., & Boernick, H. (2018). Riverbank filtration in Cairo, Egypt: part II—detailed investigation of a new riverbank filtration site with a focus on manganese. *Environmental Earth Sciences*, *77*(8), 318.

Pauss, A., Roza, A., Ledrut, M. J., Naveau, H., & Nyns, E. J. (1990). Bicarbonate determination in complex acid-base solutions by a back-titration method. *Environmental technology*, *11*(5), 469-476.

Ray, C., Grischek, T., Schubert, J., Wang, J. Z., & Speth, T. F. (2002). A perspective of riverbank filtration. *Journal-American Water Works Association*, *94*(4), 149-160.

Ray, C. (Ed.). (2002). *Riverbank filtration: understanding contaminant biogeochemistry and pathogen removal* (Vol. 14). Springer Science & Business Media.

Ray, C. (2008). Worldwide potential of riverbank filtration. *Clean Technologies and Environmental Policy*, *10*(3), 223-225.

Rickard, D. T. (1975). Kinetics and mechanism of pyrite formation at low temperatures. *American Journal of Science*, *275*(6), 636-652.

Rust, G. W. (1935). Colloidal primary copper ores at Cornwall Mines, southeastern Missouri. *The Journal of Geology*, *43*(4), 398-426.

Sawlowicz, Z. (1993). Pyrite framboids and their development: a new conceptual mechanism. *Geologische Rundschau*, *82*(1), 148-156.

Schwarzenbach, R. P., Giger, W., Hoehn, E., & Schneider, J. K. (1983). Behavior of organic compounds during infiltration of river water to groundwater. Field studies. *Environmental science & technology*, *17*(8), 472-479.

Sprenger, C., Lorenzen, G., Hülshoff, I., Grützmacher, G., Ronghang, M., & Pekdeger, A. (2011). Vulnerability of bank filtration systems to climate change. *Science of the Total Environment*, *409*(4), 655-663.

Sprenger, C., Hartog, N., Hernández, M., Vilanova, E., Grützmacher, G., Scheibler, F., & Hannappel, S. (2017). Inventory of managed aquifer recharge sites in Europe: historical development, current situation and perspectives. *Hydrogeology Journal*, *25*(6), 1909-1922.

Stuyfzand, P. J. 1989. Hydrology and water quality aspects of Rhine bank ground water in The Netherlands. *Journal of Hydrology*, *106*, 341-363.

Stuyfzand, P. J. (1998). Quality changes upon injection into anoxic aquifers in the Netherlands: Evaluation of 11 experiments. In: *Artificial Recharge Groundwater* (pp. 283-291), Balkema, Rotterdam, The Netherlands.

Stuyfzand, P. J., & Stuurman, R. J. (2006, September). Origin, distribution and chemical mass balances of non-anthropogenic, brackish and (hyper) saline groundwaters in the Netherlands. In *Proc. 1st SWIM-SWICA Joint Saltwater Intrusion Conference, Cagliari, Italy* (pp. 151-164).

Stuyfzand, P. J., Juhàsz-Holterman, M. H., & de Lange, W. J. (2006a). Riverbank filtration in the Netherlands: well fields, clogging and geochemical reactions. In: *Riverbank Filtration Hydrology* (pp. 119-153), Springer, Dordrecht, The Netherlands.

Stuyfzand, P. J., & Raat, K. J. (2010). Benefits and hurdles of using brackish groundwater as a drinking water source in the Netherlands. *Hydrogeology Journal*, *18*(1), 117-130.

Stuyfzand, P. J. (2011). Hydrogeochemical processes during riverbank filtration and artificial recharge of polluted surface waters: zonation, identification, and quantification. In: *Riverbank Filtration for Water Security in Desert Countries* (pp. 97-128), Springer, Dordrecht, The Netherlands.

Wallis, I., Prommer, H., Berg, M., Siade, A. J., Sun, J., & Kipfer, R. (2020). The river–groundwater interface as a hotspot for arsenic release. *Nature Geoscience*, *13*(4), 288-295.

Walter, A. L., Frind, E. O., Blowes, D. W., Ptacek, C. J., & Molson, J. W. (1994). Modeling of multicomponent reactive transport in groundwater: 2. Metal mobility in aquifers impacted by acidic mine tailings discharge. *Water Resources Research*, *30*(11), 3149-3158.

Wilkin, R. T., & Barnes, H. L. (1997). Formation processes of framboidal pyrite. *Geochimica et Cosmochimica Acta*, *61*(2), 323-339.

Williams, M. D., & Oostrom, M. (2000). Oxygenation of anoxic water in a fluctuating water table system: an experimental and numerical study. *Journal of Hydrology*, *230*(1-2), 70-85.

Xie, X., Wang, Y., Li, J., Yu, Q., Wu, Y., Su, C., & Duan, M. (2015). Effect of irrigation on Fe (III)–SO_4^{2-} redox cycling and arsenic mobilization in shallow groundwater from the Datong basin, China: evidence from hydrochemical monitoring and modeling. *Journal of Hydrology*, *523*, 128-138.

Zhang, Y. C., Slomp, C. P., Broers, H. P., Passier, H. F., & Van Cappellen, P. (2009). Denitrification coupled to pyrite oxidation and changes in groundwater quality in a shallow sandy aquifer. *Geochimica et Cosmochimica Acta*, *73*(22), 6716-6726.